Chest electrical impedance tomography examination, data analysis, terminology, clinical use and recommendations: consensus statement of the TRanslational EIT developmeNt stuDy group

Inéz Frerichs, Marcelo B. P. Amato, Anton H. van Kaam, David G. Tingay, Zhanqi Zhao, Bartłomiej Grychtol, Marc Bodenstein, Hervé Gagnon, Stephan H. Böhm, Eckhard Teschner, Ola Stenqvist, Tommaso Mauri, Vinicius Torsani, Luigi Camporota, Andreas Schibler, Gerhard K. Wolf, Diederik Gommers, Steffen Leonhardt, Andy Adler, TREND study group

ONLINE SUPPLEMENT 2

EIT raw images

EIT raw images

This electronic online supplement (EOS) 2 describes how raw EIT images are generated from raw EIT data acquired during EIT chest scanning. Figure E1.1 shows the sequences of all processes involved in EIT examinations and EIT data analysis for orientation.

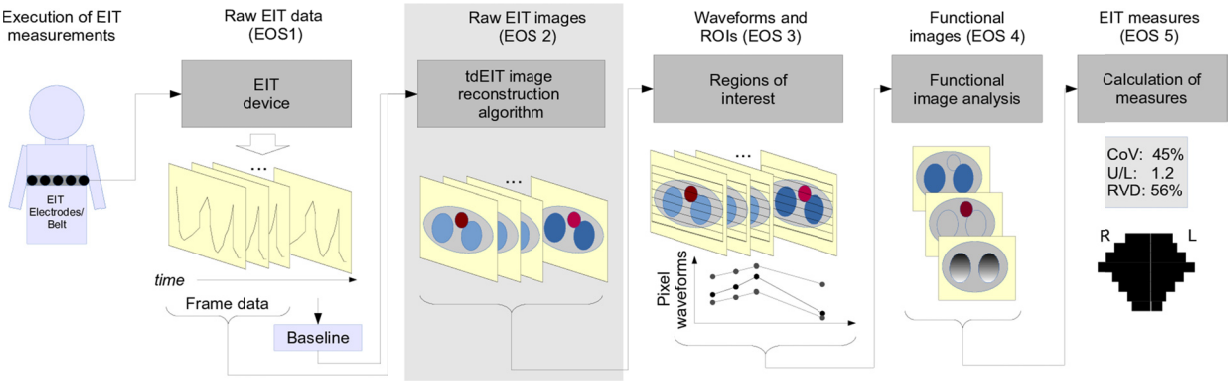

Figure E2.1. Sequence of processes involved in EIT chest examination and data analysis. EOS 2 (gray background) describes the process of raw image generation.

EIT raw data

EIT devices interact with the body using an electrical current stimulation across a set of electrodes. In a predefined sequence, current is applied to pairs of electrodes, while voltage differences are measured at all other pairs of electrodes. The set of EIT data acquired during one cycle of current applications and voltage measurements is typically called frame. One EIT data frame contains the information necessary to generate one raw image.

EIT scan rate

The number of frames (or raw images) acquired per second corresponds with the EIT scan rate. Current EIT devices offer maximum scan rates of about 40 to 50 images/s, although scan rates of 1000 images/s for industrial process tomography EIT devices have been reported (1). A larger scan rate permits observation of higher frequency physiological changes. Figure E2.2 shows a time series of EIT images obtained during one respiratory cycle. In order to avoid misrepresentation of the underlying events (aliasing), the scan rate should be larger than twice the rate of frequency content of the most rapid changes. We recommend scan rates of at least 10 images/s for monitoring of breathing and ventilation

and 25 images/s for monitoring of cardiac related physiology. Even very high frequency events such as high frequency oscillatory ventilation can be monitored by modern EIT devices (2). Further discussion of scan rates and filtering is in EOS 3.

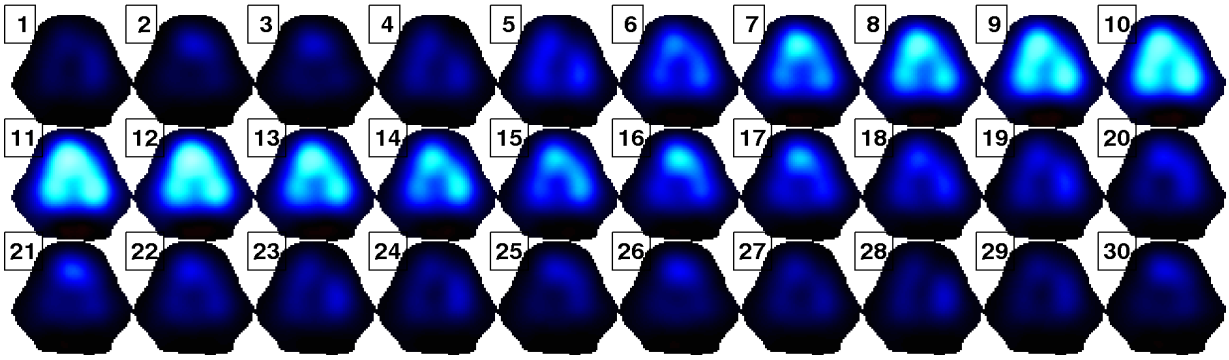

Figure E2.2. Example of EIT images acquired at a scan rate of 13 images/s (data from a mechanically ventilated pig with experimental lung injury (3) acquired with the Goe-MF II device (CareFusion, Höchberg, Germany)). EIT images frames (numbered) show subsequent frames from left to right during a single respiratory cycle.

EIT tissue sensitivity

EIT is sensitive to changes in electrical conductivity properties of tissue at the stimulation frequency. Conductivity is a bulk property of materials, and is measured in Siemens per meter (S/m) with a range of 0.042 (inflated lung), 0.11 (deflated lung), 0.48 (heart) and 0.60 (blood) (4, 5). Resistivity (in Ω·m) is the inverse of conductivity. At low frequencies, electrical current flows primarily through conductive pathways (in the body, regions of high ionic conductivity). As the frequency increases, oscillating currents (also called displacement currents) are able to travel across otherwise insulating barriers such as cell membranes. At a specific current stimulation frequency the conduction properties of tissue are described by the admittivity (S/m) and its inverse, the impedivity (Ω·m). To date EIT systems have operated at relatively low frequencies (≤250 kHz), where current flow in tissue is mostly conductive, and the resistivity and impedivity are roughly equal (which explains how these terms are sometimes conflated). The measurement of tissue electrical properties at multiple higher frequencies is called electrical impedance spectroscopy and serves a role in characterizing properties of tissue samples (6-9). This method does not provide images, and is typically not useful for real-time imaging, since its acquisition rates are relatively low compared to EIT.

The conductivity properties of most tissues are relatively well known *ex vivo* (e.g. (10)). The main factor in tissue is the fluid content, such that body fluids are conductive and gases resistive. Since time-difference EIT (tdEIT) is a dynamic modality, it is sensitive to changes in conductivity rather than the absolute conductivity level. Physiological changes occur primarily due to the movements of body fluids (e.g. blood in blood vessels) and gases (e.g. air in the lungs). For example, as the lungs inflate, electrical current must pass through the parenchyma which is more widely spaced by the incoming air. Unfortunately, to our knowledge, there are no good *in vivo* measurements of the lung conductivity as a function of inflation; however, most models assume a linear relationship between resistivity and lung air content (11). Changes in fluid content may be pulsatile (at the cardiac frequency) or more slowly, due to intravascular or extravascular fluid accumulation.

The impedance values measured by EIT are very sensitive to the shape and movement. Thus, the EIT signal in the heart region is a combination of the effect of blood volume changes in the heart chambers, as well as the movement of the heart in the thoracic cavity (12). EIT signals are similarly sensitive to changes in electrode position (13), body posture (14-20), and electrode contact impedance (21, 22).

EIT position sensitivity

EIT is most sensitive to conductivity changes in the electrode plane, and has decreasing sensitivity to off-plane effects. Note, however, that EIT does not provide a "slice" such as from CT or MRI images. Instead, there is a gradual decrease in sensitivity with off-plane distance. The decrease in sensitivity depends on the distance from the body surface. Close to the skin, the off-plane sensitivity is low, while for conductivity changes near the thorax centre, sensitivity is roughly half the chest width. Figure E2.3 explores this effect. Using a finite element model (FEM), objects at different positions within the electrode plane are simulated to move up- and downwards and the sensitivity calculated.

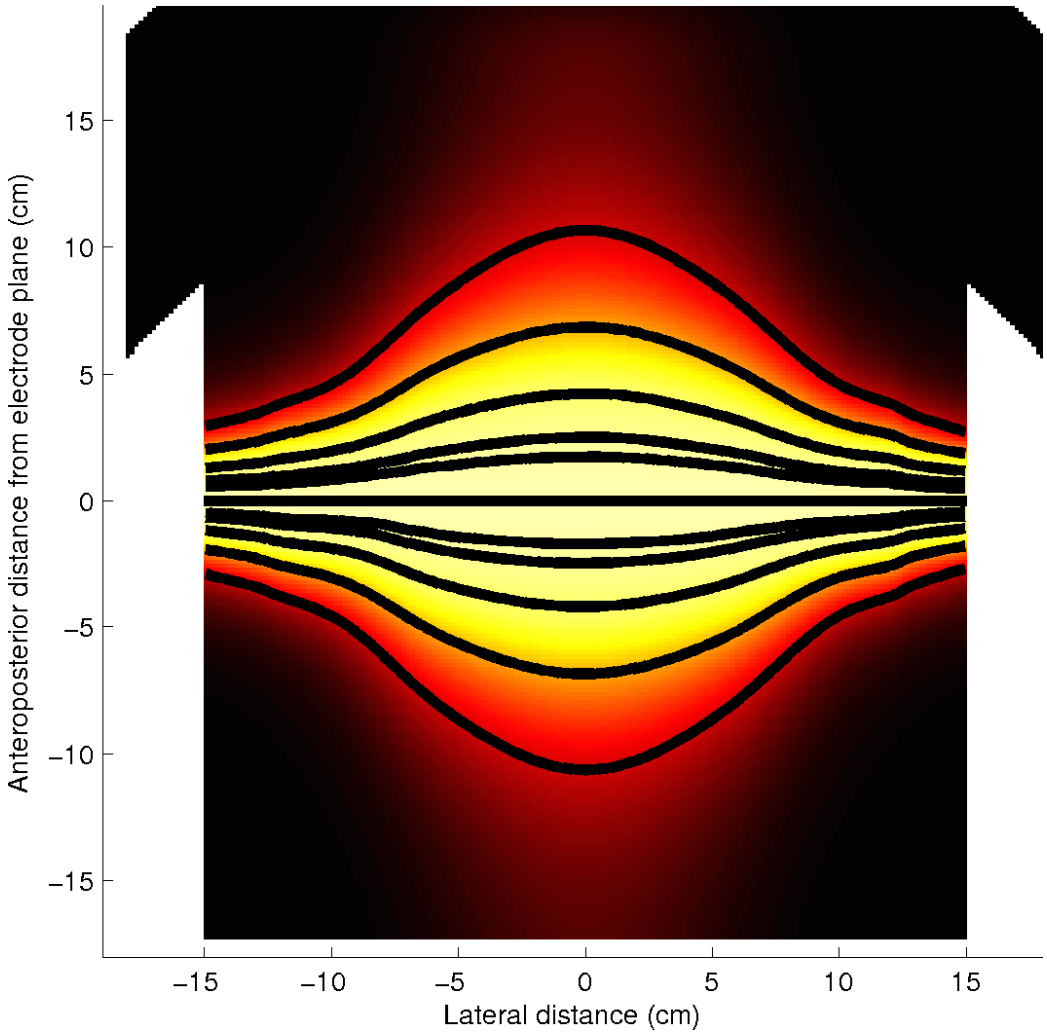

Figure E2.3. Frontal plane showing the relative vertical sensitivity of EIT measurements as a function of the position above and below the electrode plane. Color intensity (black = 0) corresponds to sensitivity. Contour lines indicate regions of equal sensitivity. From the electrode plane lines indicate 95%, 90%, 75%, 50% and 25% sensitivity. Data were calculated from a finite element mesh of the human thorax with an adjacent stimulation and measurement pattern. In each vertical slice, sensitivity is normalized to its value on the electrode plane.

EIT image reconstruction

Using the measured voltages, the process of generating an image is called "image reconstruction". Typically, an image of the 2D slice through the electrode plane is reconstructed. So far, the main image reconstruction framework used is tdEIT, used in all clinical and the vast majority of experimental studies. tdEIT reconstructs an image of the change in tissue properties between a baseline (or reference) measurement frame (V_{ref}) and the measurement frame at the current time (V_t). V_{ref} is chosen to represent a physiologically

stable or relevant instant (see below). Since the meaning of an EIT image depends so centrally on the V_{ref} chosen, it is essential to describe its choice when reporting results.

Alternative image reconstruction frameworks

While all clinical results to date have been reconstructed using tdEIT, there are two other frameworks for EIT image reconstruction which are active areas of research, and may see experimental use in the near future, but are currently insufficiently robust for chest EIT:

- frequency-difference EIT (fdEIT), which is sensitive to the difference in tissue properties between stimulation frequencies. fdEIT uses special EIT hardware capable of stimulating the body with electric current at two or more frequencies. Since the electrical conductivity of tissues vary with frequencies (current may travel across cell membranes rather than around it), the multifrequency measurements reflect these differences (23, 24). fdEIT uses the similar reconstruction algorithms to tdEIT, but images represent the difference in tissue properties between frequencies rather than between V_{ref} and the current time. fdEIT has considerable promise, but has seen relatively less experimental evaluation.
- absolute imaging or absolute EIT (aEIT) calculates an image of the electrical tissue properties at a given time. Thus it does not require a V_{ref}, since each image represents the tissue properties at the time of the measurement. aEIT is routine in the analogous geophysical method; however, chest EIT presents some key challenges which have not been satisfactorily overcome by current reconstruction algorithms. First, the regions of interest (lungs) are relatively deep compared to the electrode spacing, and thus exhibit relatively low sensitivity. Next, the electrode contact and placement in chest EIT are subject to uncertainties due to sweat, contact quality, position inaccuracies and movement due to breathing and posture change. Given these challenges, aEIT has not yet seen significant clinical or experimental use.

Formulation of EIT image reconstruction

Time-difference EIT imaging

tdEIT imaging calculates an image of the impedance changes between two points in time, and is the most widespread and robust mode of image reconstruction. Since many physiological phenomena like lung ventilation and perfusion are periodic, their time-dependent changes can thus be determined by tdEIT.

tdEIT reconstruction may be understood as calculating an inverse sensitivity function. Given a tissue properties P_t at time t and properties P_{ref} during the baseline measurement,

then difference EIT is concerned with the change in tissue properties ΔP. During these times, corresponding measurements M_t and M_{ref} are made, from which a change in measurements ΔM is calculated (some reconstruction algorithms normalize this value). The sensitivity of the EIT system, S (also called the Jacobian in the literature), relates

$$\Delta M = S \Delta P$$

where the matrix S describes how some EIT measurements are more sensitive to changes in some image regions than others. In order to reconstruct an EIT image, we want to calculate ΔP from ΔM, using a reconstruction matrix R such that

$$\Delta P = R \Delta M.$$

Here, R is a pseudo-inverse of S. Because of the low sensitivity of the diffusive propagation of electrical current, EIT is an *inverse problem* and S is non-invertible. Instead, various reconstruction algorithms calculate an approximate inverse; however, reconstruction algorithms are required to choose a compromise between image features such as resolution and the ability to suppress noise.

Thus, tdEIT calculates an estimate of the change in tissue properties

$$\Delta P = P_t - P_{ref}$$

between the current and the baseline frame. Correct interpretation of these images depends on the definition of the baseline frame.

Development of new algorithms is an active field in EIT research with advances in image quality achieved by using, e.g. a-priori anatomical information. For an introduction to these algorithm developments, see (25-27).

Frequency- vs. time-difference imaging

fdEIT imaging calculates an image of the change in tissue properties between measurements made at the same time, but at two different electrical stimulation frequencies. Mathematically, fdEIT and tdEIT are formulated similarly, except that

$$\Delta P = P_a - P_b,$$

$$\Delta M = M_a - M_b$$

where a and b represent the two stimulation frequencies. Voltages are normally scaled and normalized in practice. fdEIT systems can be constructed to make the electrical measurements at exactly the same times, or in rapid succession. The frequencies may be chosen such that an electrical *dispersion* occurs between them. For example, at the higher frequency, current may pass through cell walls and through the cells, while this may not occur at the lower frequency. fdEIT images can thus be interpreted as an image of the distribution of tissue types whose electrical properties change most between the frequencies.

Absolute vs. time-difference imaging

aEIT seeks to calculate an image of the actual conductivity distribution within a body based on a single set of measurements. aEIT thus does not require a baseline measurement frame. Several groups are actively working on aEIT reconstruction algorithms, but it is not sufficiently robust for experimental or clinical use. aEIT approaches are challenging in medical applications because: first, EIT is highly sensitive to exact knowledge of the boundary shape and electrode position, which is not easily available on the chest (which moves with breathing and posture change) (28). Also, the higher electrical simulation frequencies used in medical EIT are more susceptible to various types of electronic inaccuracies. Additionally, aEIT is inherently non-linear, and its solutions require far more computation than those of linear tdEIT.

Image reconstruction requirements

As indicated the mathematics of developing an EIT reconstruction requires performing compromises in the selection of a pseudo-inverse. In order to select between the many proposed algorithms, work has been done to identify figures of merit to evaluate algorithm performance (25, 29, 30). Such work allows selection of appropriate image reconstruction to best match an application requirement.

Based on the consensus reported in (25), Figure E2.4 illustrates the developed figures of merit; an ideal reconstruction algorithm should exhibit (in order of importance):

- uniform *amplitude response* (i.e. a small contrast of given size should result in the same average image amplitude at any position in the imaging plane)
- small and uniform *position error* (i.e. a small contrast should be reconstructed in the correct position)
- high and uniform *resolution* (i.e. a small contrast should be reconstructed as a small region, in order to allow distinguishing of nearby changes; however, resolution should be uniform to avoid misinterpretation of contrasts in different regions)
- small *ringing artifacts* (where "ringing" means image regions with a change inverse to the underlying tissue properties)
- low *noise amplification* (i.e. the effect of electronic noise in measurements should be minimized in the reconstructed images)
- low *shape deformation* (i.e. the shape of regions should be preserved – except for blurring)
- small sensitivity to electrode and boundary movement.

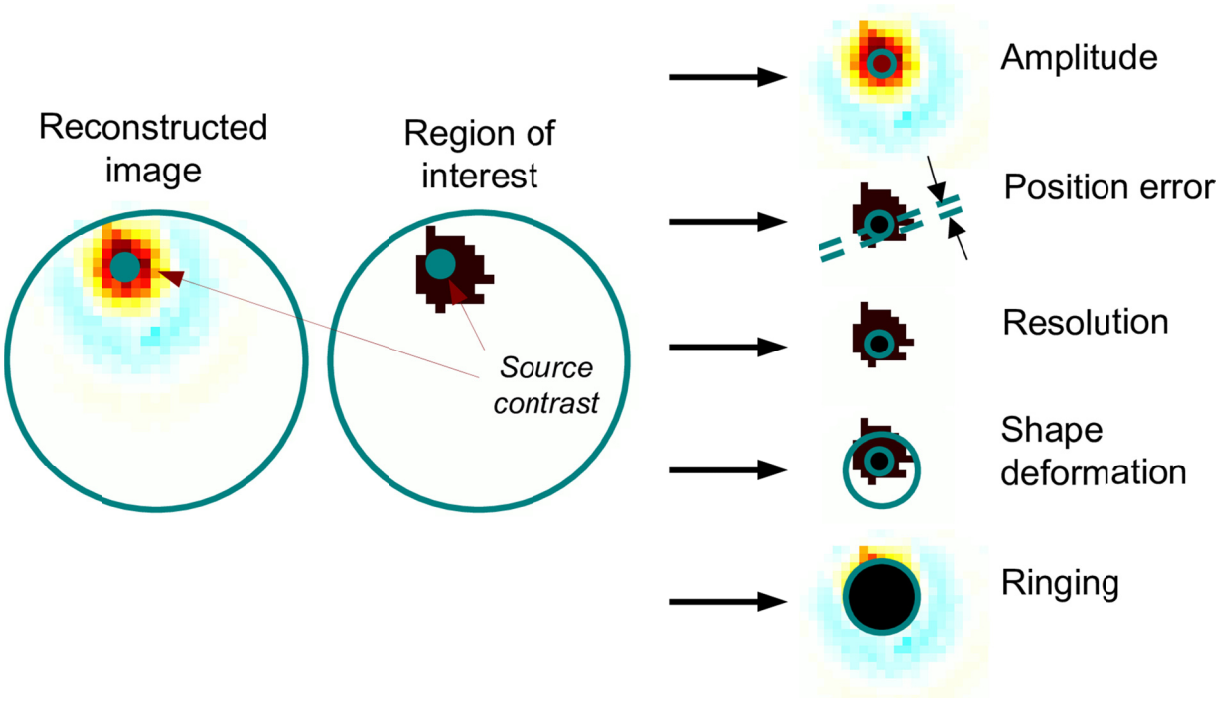

Figure E2.4. Figures of merit for EIT reconstructions (25). From a source contrast of known position (simulated or measured), an image is reconstructed (left) and the ROI determined corresponding to image regions above 25% maximum amplitude (center). Using these data: 1) the amplitude is the sum of all image pixel amplitudes, 2) the position error is the distance from the source centre to ROI centre, 3) the resolution is the size of the ROI, 4) the Shape deformation is the ROI area outside of region in a circle of the same area as the ROI, and 5) the Ringing is the relative amplitude of the inverted area of the image.

Impact of image reconstruction on image appearance

The mathematical problems underlying EIT image reconstruction are subtle and have inspired and challenged mathematicians and computational scientists for a third of a century (31). Novel and interesting reconstruction approaches are explored in the mathematical, engineering and physics literature. We would like to address here a few aspects of image reconstruction algorithms relevant also for medical use in chest EIT imaging.

In Figure E2.5, a sample of tdEIT common reconstruction algorithm approaches is shown. In order to compare algorithms fairly, this figure was calculated by imposing a circular shape assumption for all models.

First (Figure E2.5, top left) is the Sheffield backprojection algorithm (SBP), developed for the first EIT device, the Sheffield Mark I in the mid 80´s of the last century, and described by (32, 33). SBP has been very widely used; however, it has some inaccuracies due to its formulation – driven by the limitations of computer hardware in the early 1980s.

Specifically, it is limited by the use of an inadequate, 2D sensitivity model. From the point of view of interpretation, SBP can display streak-like artefacts, which point toward the boundary. Another limitation is the assumption of a circular geometry for the electrodes and the body. Nonetheless, in spite of these limitations, SBP works surprisingly well (30) which allows the findings of a great number of EIT studies to be considered valid.

Next, (Figure E2.5, top right) is the GREIT algorithm (25) developed by a consensus group of EIT experts. GREIT is based on a mathematical optimization of reconstructed images against a set of defined figure of merit parameters.

Next, (Figure E2.5, bottom left) is a regularized linear Gauss-Newton (GN) reconstruction. The image is calculated to match the measured data and a "regularization" (or smoothness) constraint. The choice of regularization constraint is a rich research area; GN algorithms allow a trade-off between noise immunity, image resolution, and fidelity to various image shape constraints (34, 35).

Last, (Figure E2.5, bottom right) is an example of a non-linear tdEIT algorithm. This specific image uses a Total Variation (TV) constraint (36) which enhances edges between regions in the image. TV approaches do not show the blur inherent with linear algorithms, but have been criticised as showing the appearance of greater resolution than is actually available from the data (36).

Comparing image reconstruction algorithms

Each EIT image reconstruction algorithms is best understood as a framework with many "ingredients". Each ingredient can be varied, and will have an effect on the accuracy and reliability of the calculated images. In the following subsections, we consider the effects of four algorithm parameters: shape, orientation, background, and noise performance.

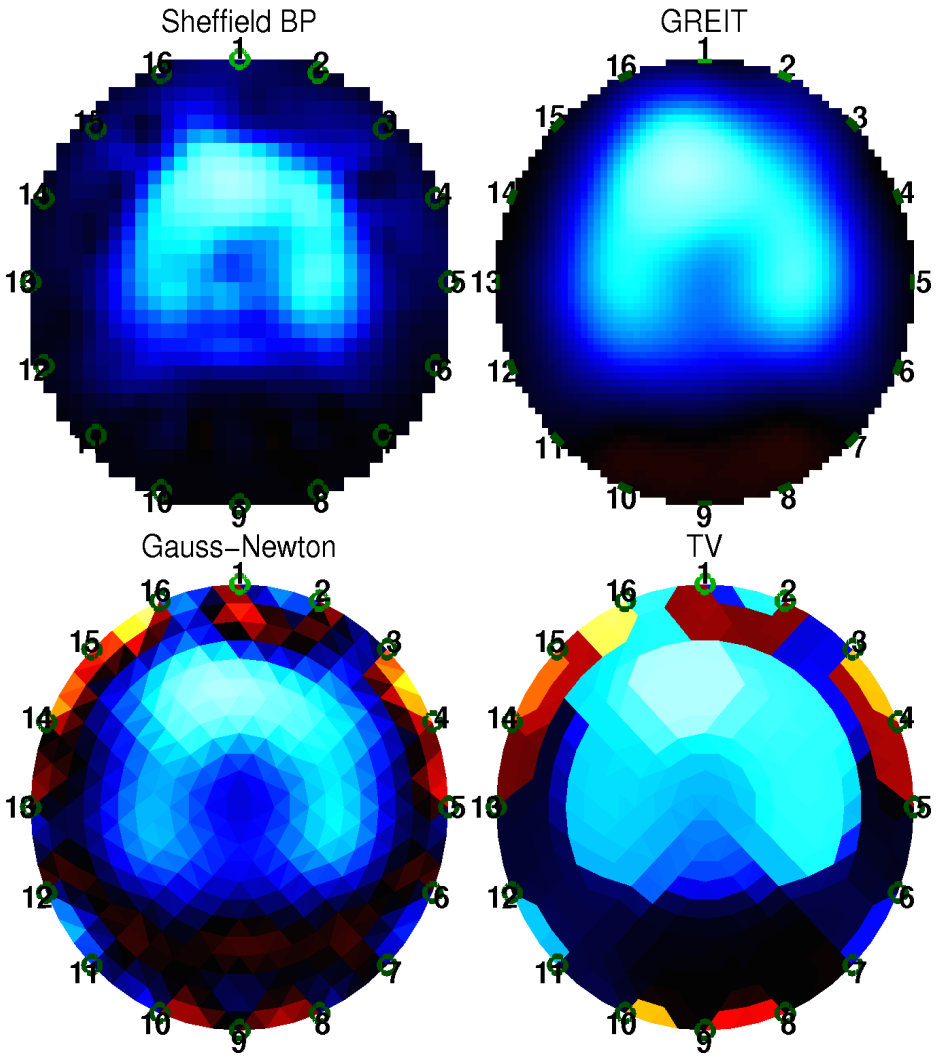

Figure E2.5. Examples of image reconstruction algorithms applied to an identical EIT data set (3). BP, backprojection; GREIT, Graz consensus; GN, Gauss-Newton; TV, Total Variation.

Image reconstruction shape

The earliest EIT images assumed that electrodes were placed on a circular plane on a cylindrical body. These round images were obtained using the so-far most widespread image reconstruction procedure, SBP. The computational advances in the 1990s made it relatively straightforward to model the contour of the anatomical form of the chest. Figure E2.6 illustrates the effect of the choice of anatomical shape; an image of tidal breathing is reconstructed on four different models. Images illustrate that the ability of EIT to separate the lung regions is compromised when the model is clearly wrong (ellipse and adult human).

Undoubtedly, the best selection is of a model shape which exactly matches the subject. However, in many cases, this is not available, because a scan of the subject has not been performed, and also because thorax shape changes with posture. In these cases the best shape match should be chosen. A study of the required accuracy of shape matching

(37) suggested that an area mismatch of less than 4% corresponded to accurate reconstructed images.

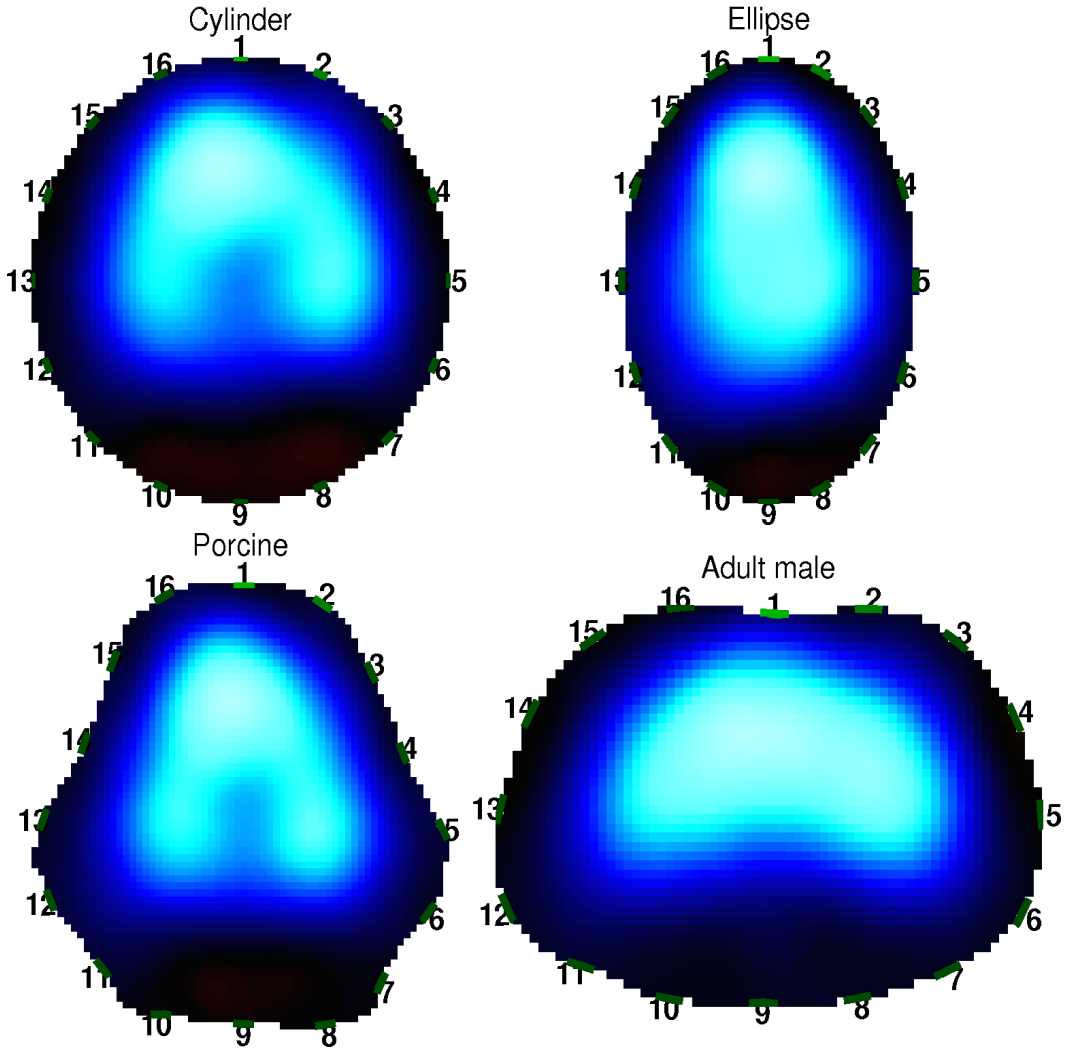

Figure E2.6. Algorithm shapes. EIT data obtained from a lung-healthy mechanically ventilated piglet (3) representing tidal ventilation (end-inspiration – end-expiration) were reconstructed using the GREIT algorithm with various assumed thorax shapes. *1*: Cylindrical thorax (top left) *2*: Elliptical thorax (top right) *3*: Porcine shape thorax (Generic) (bottom left) *4*: Adult human shape thorax (bottom right). The porcine shape was not specifically adapted to the thorax shape of the specific animal. Note the relative deformations of the reconstructed form.

Image reconstruction noise performance

EIT algorithms implicitly make assumptions about the level of random noise (interference) in the raw data. When the noise level is assumed to be high, an algorithm will smooth (or blur) the image to supress such noise. However, if data have low levels of noise, it is appropriate to let the algorithm reduce blurring which allows better spatial separation of image regions. One common way to measure the assumed noise level of the algorithm is using the Noise

Figure parameter (34). In several papers, the value of a parameter or "hyperparameter" is adjusted to achieve a similar effect. Using the porcine shape Figure E2.7 shows the same data as in Figure E2.6 reconstructed with the GREIT algorithm with different levels of assumed noise.

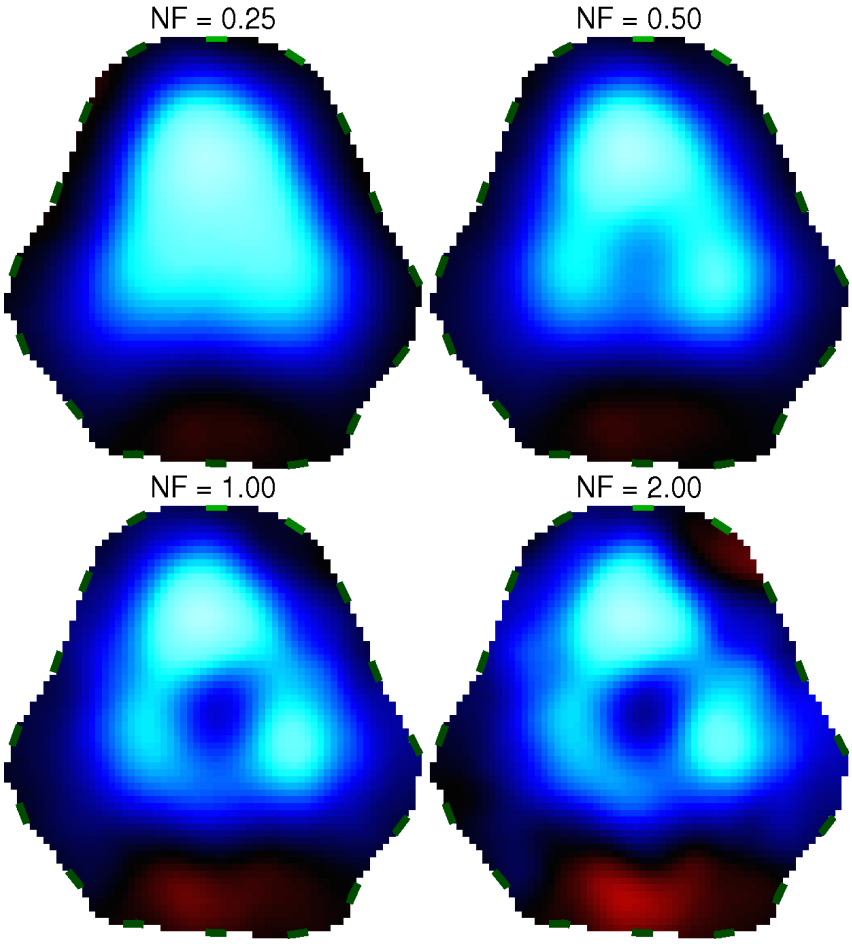

Figure E2.7. Smoothing and noise suppression in image reconstruction. EIT data obtained from a lung-healthy mechanically ventilated piglet (3) representing tidal ventilation (end-inspiration – end-expiration) were reconstructed using the GREIT algorithm with various assumed noise levels. Images are shown corresponding to an algorithm NF (Noise Figure) of 0.25, 0.5, 1.0 and 2.0. At higher NF values, there is reduced spatial blurring and regions become more separate. The top right image is the same as the one shown in Figure E2.6.

Image reconstruction background

As indicated, tdEIT algorithms reconstruct a change in impedance distribution, between a measurement, M_t and a baseline measurement, M_{ref}. Reconstruction then uses a sensitivity matrix, S, calculated at the assumed conditions during M_{ref}. The assumed impedance distribution at M_{ref}, is typically called the "background" distribution. Almost all tdEIT algorithms have made the simplest assumption, that the background is homogeneous; however, for the thorax, this assumption is clearly false. Some recent algorithm work

considers non-uniform background conductivities. In these images, the contrast in the lung region is enhanced because it accounts for the inherent lower sensitivity in low-conductivity lungs. Figure E2.8 shows images of tidal breathing with different values of the assumed background conductivity of the lungs with respect to the average of other thoracic tissues.

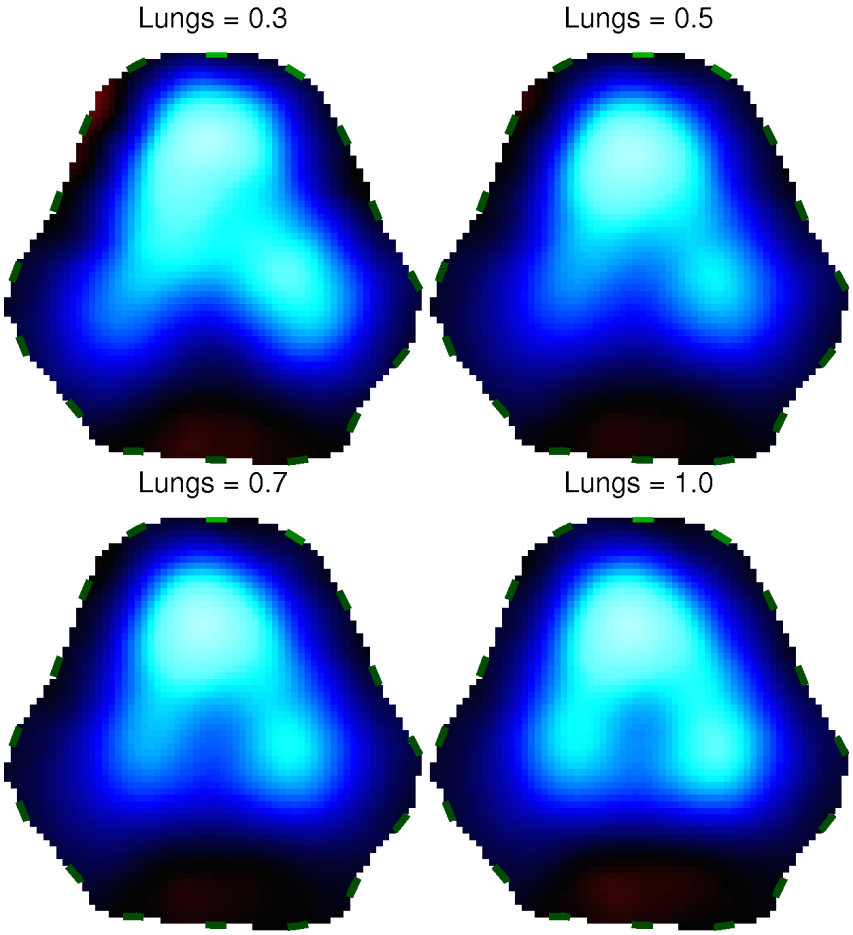

Figure E2.8. Effect of image reconstruction background distribution. EIT data obtained from a lung-healthy mechanically ventilated piglet (3) representing tidal ventilation (end-inspiration – end-expiration) were reconstructed using the GREIT algorithm with models of the lung region conductivity with respect to the average of other thoracic tissues.

Pixel vs. finite element grid

EIT images have typically been represented in two ways, as a pixel grid or on a triangular representation (Figure E2.9). A representation on a pixel grid means that all image elements are the same size, and thus the calculation of functional parameters do not need to scale image elements by size. A representation on a triangular grid is common when the underlying algorithm uses a finite element mesh. In this case, image elements are typically of different sizes, but can often approximate the boundary shape more accurately. We recommend the use of pixel grid; since EIT is a functional modality, the ease of representing functional parameters is more useful than the ability to represent the boundary shape.

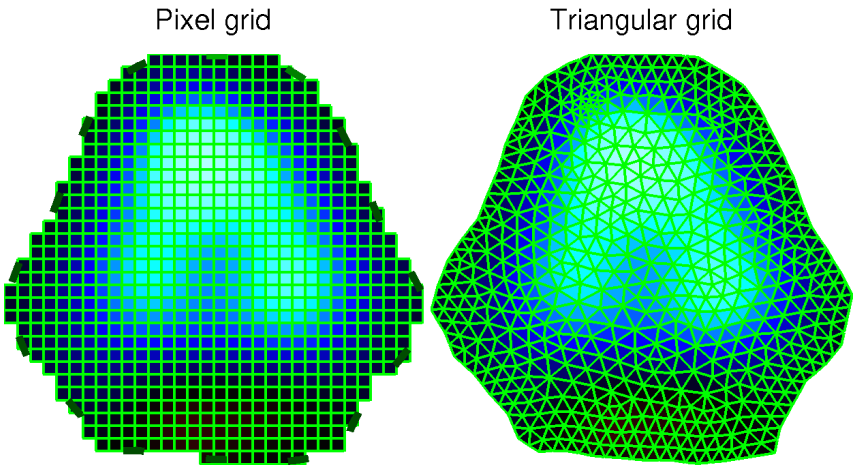

Figure E2.9. Representation of EIT images. *Left*: EIT reconstructed image parameters represent pixels in a matrix (green); *Right*: EIT reconstructed image parameters represent triangular regions based on a finite element mesh (green).

Colour mapping

The color coding of EIT images is not unified. Different color representations have been used by various research groups and vendors of EIT technology. Perhaps the most common are the grey and "jet" color maps but many other representations have been used. Figure E2.10 shows some commonly used color mappings.

We identify specific issues with the choice of EIT color coding. First, for difference images, there is a zero, which represents no change in the images. This zero has a clear representation in some image color codings. Positive and negative changes from this zero are then defined. However, some other color schemes do not define the zero color and only the color limits representing the maximum and minimum image values are provided.

Two choices have been made to modify the visual strength of these conductivity changes. First, the choice of colors may modulate the appearance of positive and negative changes, and, second, the use of a uniform region which compresses all changes less than a certain level to be represented as the zero color. In the absence of consensus, we recommend that color maps be defined and clarified for each use.

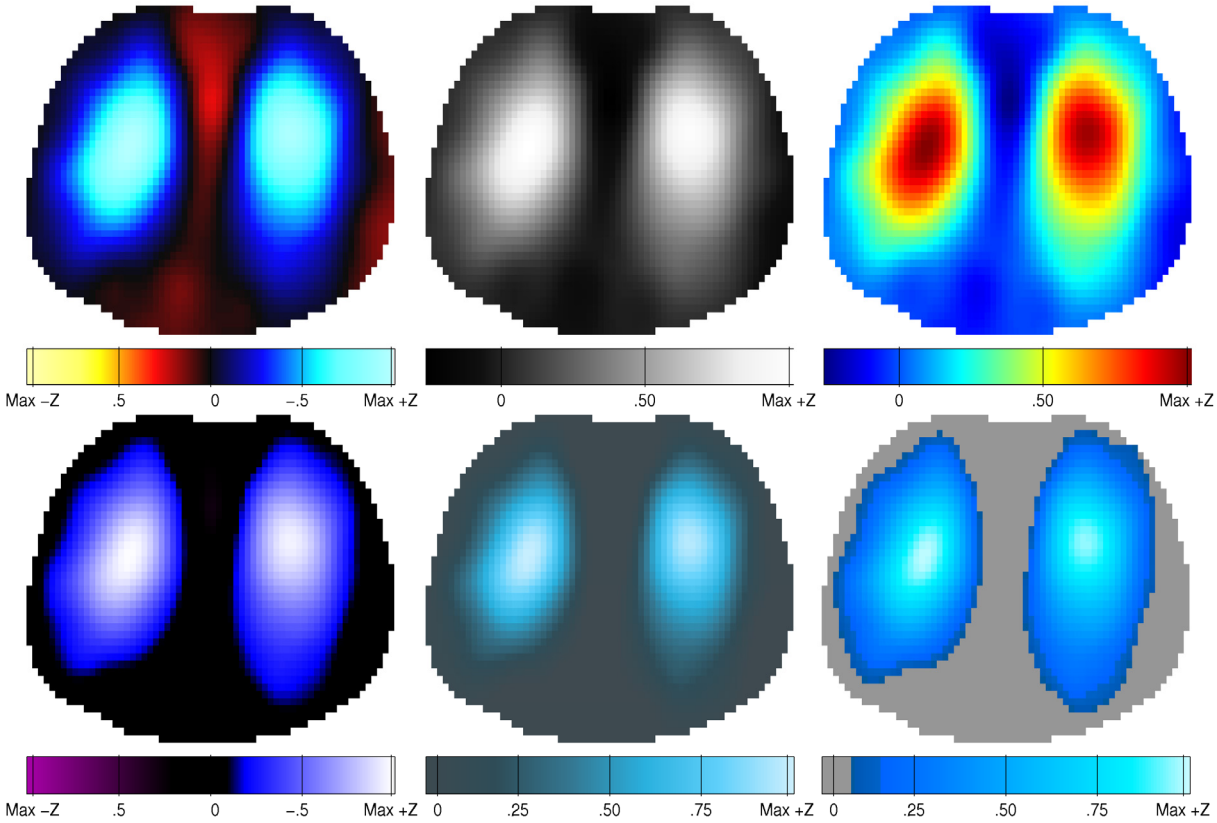

Figure E2.10. Common color coding schemes used in EIT lung images, based on academic publications (top row) and EIT system vendors (bottom row). The representation of impedance increase (Z↑ or +Z) and impedance decrease (Z↓ or –Z) are described.

Top left: *Blue-white-red,* showing Z↑ as blue, Z↓ as red, and zero as white.

Top middle: *Gray*, representing Z↑ as white, and Z↓ as black. This color scheme does not define a fixed color value for no change (zero).

Top right: *Jet*, defined from the definition in Matlab (Mathworks, Nantick, MA, USA). representing Z↑ as red, and Z↓ as blue. This color scheme does not define a fixed color value for no change (zero).

Bottom left: *Draeger,* representing Z↑ blue-white, Z↓ as purple, and zero as black with a uniform color region around zero.

Bottom middle: *Swisstom,* representing Z↑ as blue-white, and zero as blue-grey with a uniform color region at and above zero. Colors for Z↓ are not defined.

Bottom right: *Timpel,* representing Z↑ as blue-white, and zero as grey black with a uniform color region at and above zero. Colors for Z↓ are not defined.

(The raw EIT data used to generate the images with different color coding in this figure were acquired in a healthy human subject during tidal breathing and originate from (38).)

Image reconstruction orientation

The orientation of EIT images is identical with the images generated by established medical imaging modalities like computed tomography with the subject right side on the left side of the image and with anterior at the top of the image. In much of the older EIT literature (before 2000), it was common to represent the EIT image horizontally reversed, that is with the subject anterior shown at the bottom of the image (Figure E2.11).

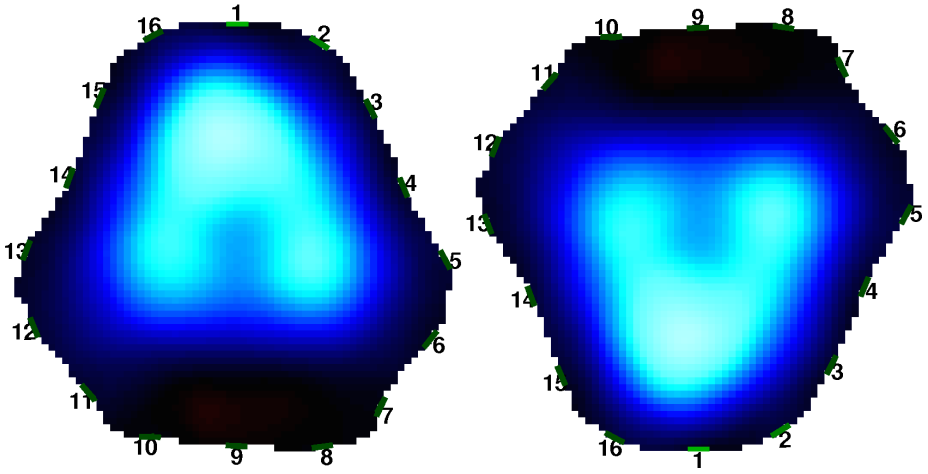

Figure E2.11. Image orientation. Modern EIT systems use a medical image orientation (*left*) while some older systems were vertically flipped (*right*). (Data is from (3)).

Selection of tdEIT baseline measurement

As mentioned, tdEIT reconstructs a change in volume distribution between a baseline measurement and a current measurement. Therefore, interpretation of the image requires the knowledge of what is "happening" in terms of physiology at both measurement points. While the "current" measurement normally represents a point in time, the "baseline" measurement represents either another single point in time or the mean value of a period of time. It is thus essential to specify how the baseline measurement is selected. Various strategies have been developed to select a baseline measurement; however, a small number of approaches are most commonly used, and are discussed here.

Baseline as a mean of EIT data

The most common strategy is to simply use the mean of all measurements as the baseline image. This approach has two benefits. It is simple and robust. It can be applied to all types of breathing patterns, and is less affected by sighs, coughs, other "unusual" breathing patterns, or signal disturbances. However, the main disadvantage is that images will be represented as both positive and negative. It is generally more difficult to visually interpret these images, as the "zero" image does not correspond to any particularly physiologically

significant time (typically it will represent lung midcapacity above end-expiratory lung volume). Another disadvantage is that the global mean is only available after the complete recording. This strategy is thus only suitable for post-processing of data. Figure E2.12 shows how the appearance of EIT images is influenced when mean EIT measurement data are used as baseline.

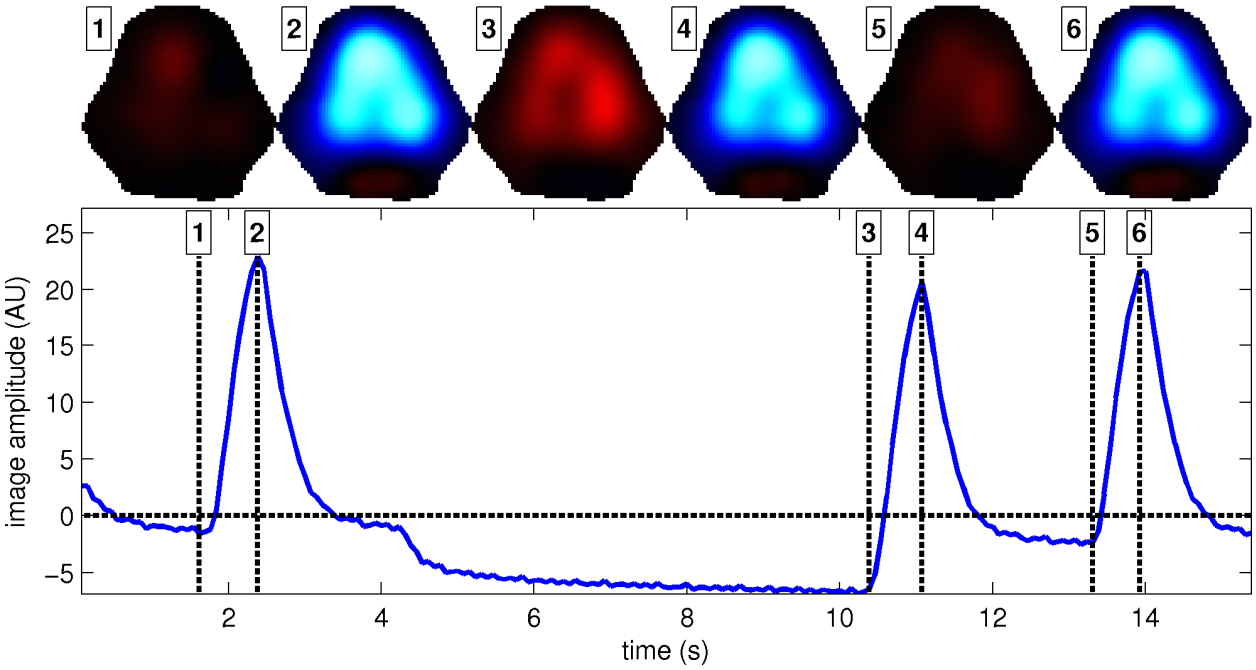

Figure E2.12. EIT images and the global EIT waveform for the baseline based on the mean value of acquired EIT data. Top row, images (using a blue-black-red color coding) corresponding to the indicated times (dashed lines). Bottom row: average image value vs. time for the shown three breaths (data from (3)).

Baseline at end-expiration or end-inspiration

Another common strategy is to select a physiologically meaningful event as the baseline scan. This is typically the end of expiration or inspiration. The advantage is that images then have a more natural physiological interpretation (Figures E2.13 and E2.14). The chosen baseline scan may be either a single instant, or an average of all end-expiration in the recording. The baseline may be chosen manually or with automated software.

One disadvantage with this strategy is that "unusual" breathing patterns, such coughs or sighs or other signal disturbances, can make identification of a true physiological event difficult. Additionally, this strategy is most suitable for post-processing of data.

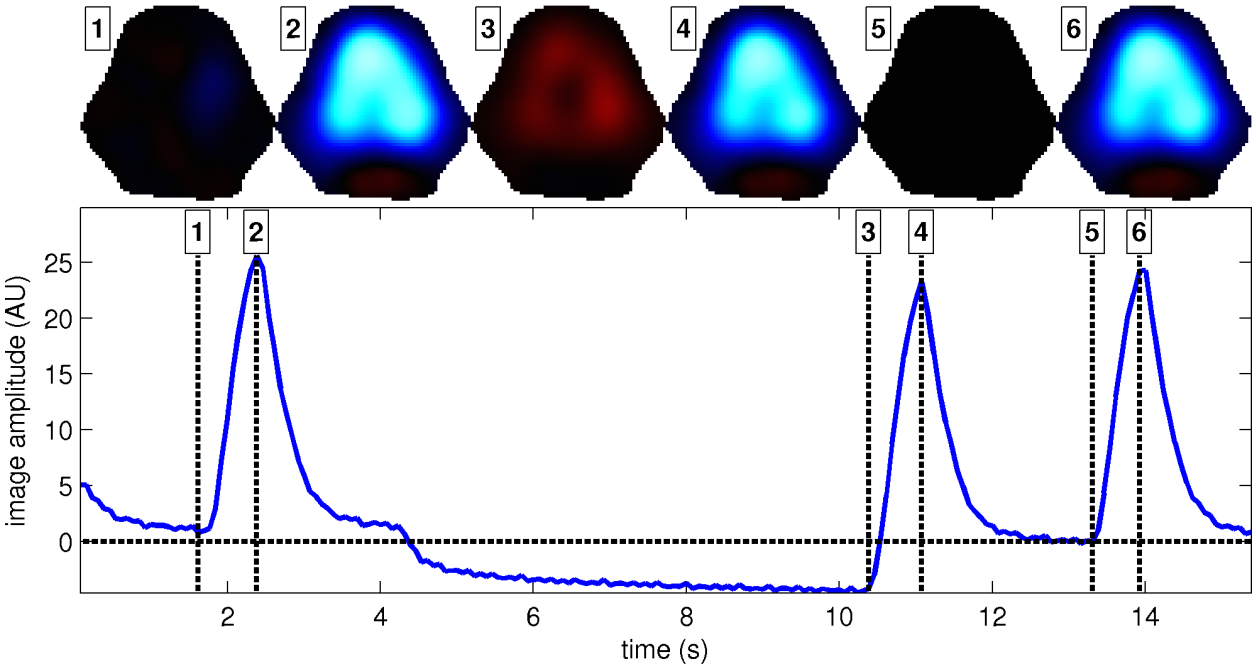

Figure E2.13. EIT images and the global EIT waveform for the "end-expiratory" baseline measurement. Top row, images (using a blue-black-red color coding) corresponding to the indicated times (dashed lines). Bottom row: average image value vs. time for the shown three breaths (data from (3)).

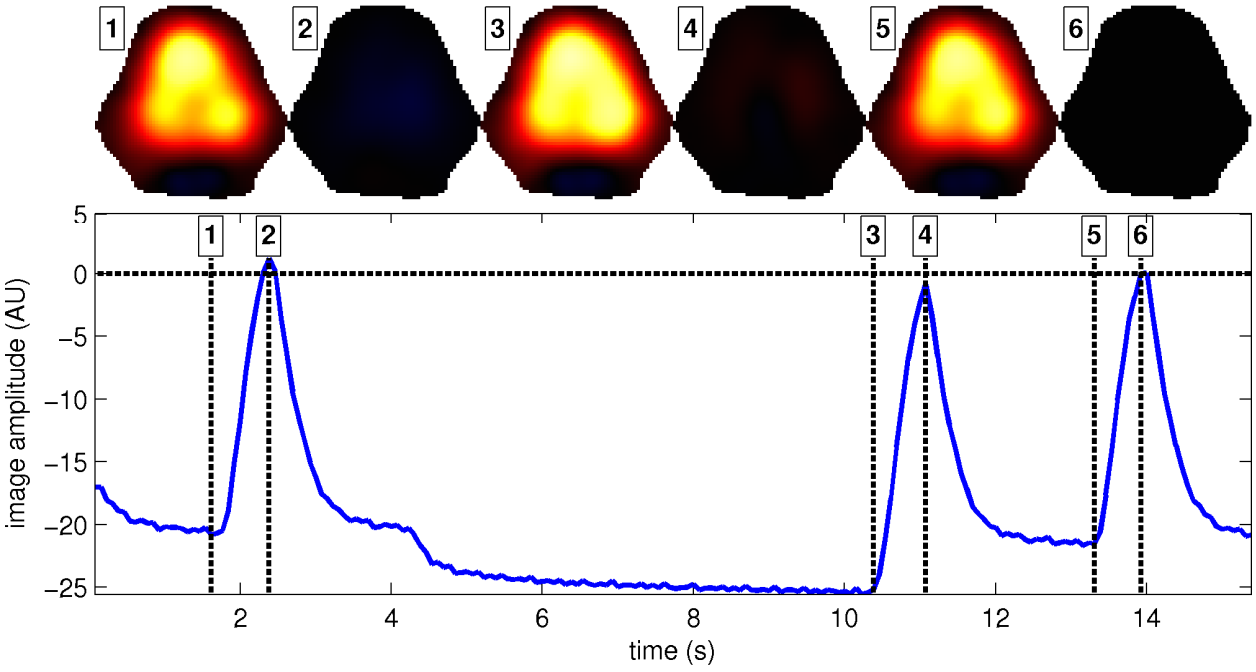

Figure E2.14. EIT images and the global EIT waveform for the "end-inspiratory" baseline measurement. Top row, images (using a blue-black-red color coding) corresponding to the indicated times (dashed lines). Bottom row: average image value vs. time for the shown three breaths (data from (3)).

Baseline from moving averages

In cases where it is essential to analyse EIT data on-line, a dynamic selection of the baseline scan is required. Clearly, such a strategy must use only previous data, and must thus be updated dynamically. In this case, the most natural extension of the mean scan baseline strategy is a dynamic mean. As an example, in Figure E2.15, the mean of the previous 2 s of data is used. However, in practice a longer interval is used. The dynamic mean has many of the advantages and disadvantages of the mean scan. Additionally, it can show temporary differences when the patient state changes. For example, when PEEP or patient posture changes, the dynamic mean will slowly adjust to the new level at which point it will "forget" the previous state.

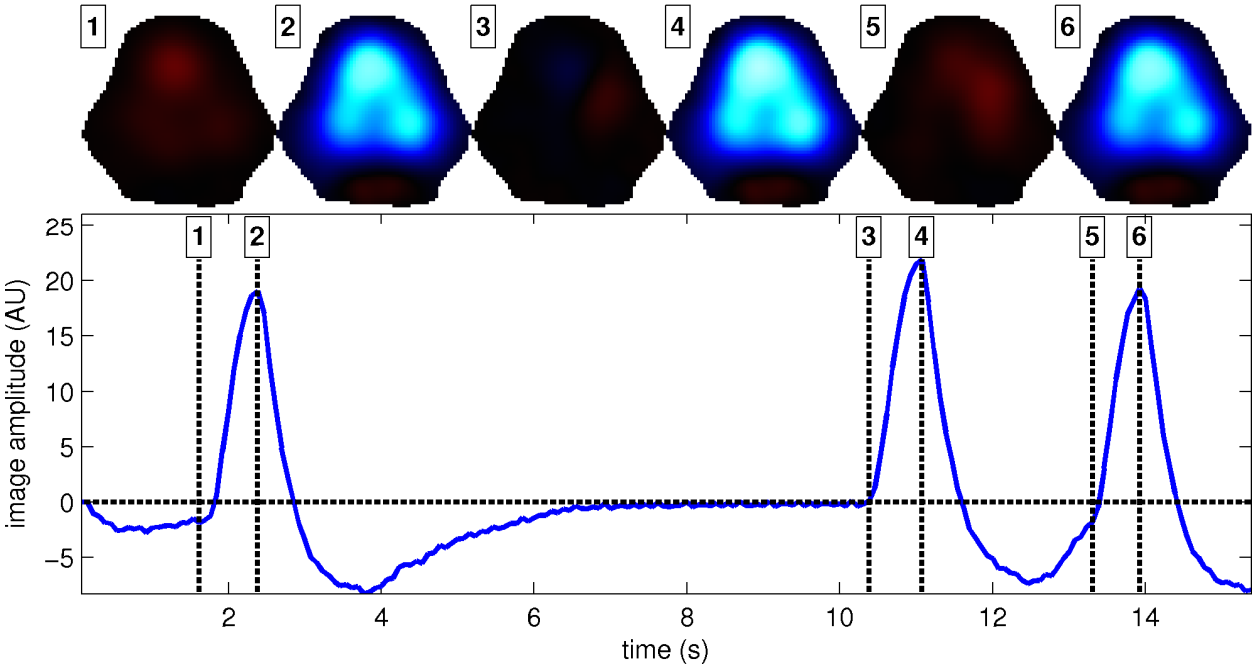

Figure E2.15. EIT images and the global EIT waveform for the "dynamic mean" baseline measurement, in which the mean is based on the last 2s of the signal. Top row, images (using a blue-black-red color coding) corresponding to the indicated times (dashed lines). Bottom row: average image value vs. time for the shown three breaths (data from (3)).

The natural extension of the end-expiratory strategy for on-line analysis is the dynamic end-expiratory baseline. In this case, the average of the previous *N* end-expirations is chosen (Figure E2.16). This strategy has the advantages of the dynamic mean scan, but also has a more natural physiological interpretation since the baseline scan corresponds to a natural physiological interpretation.

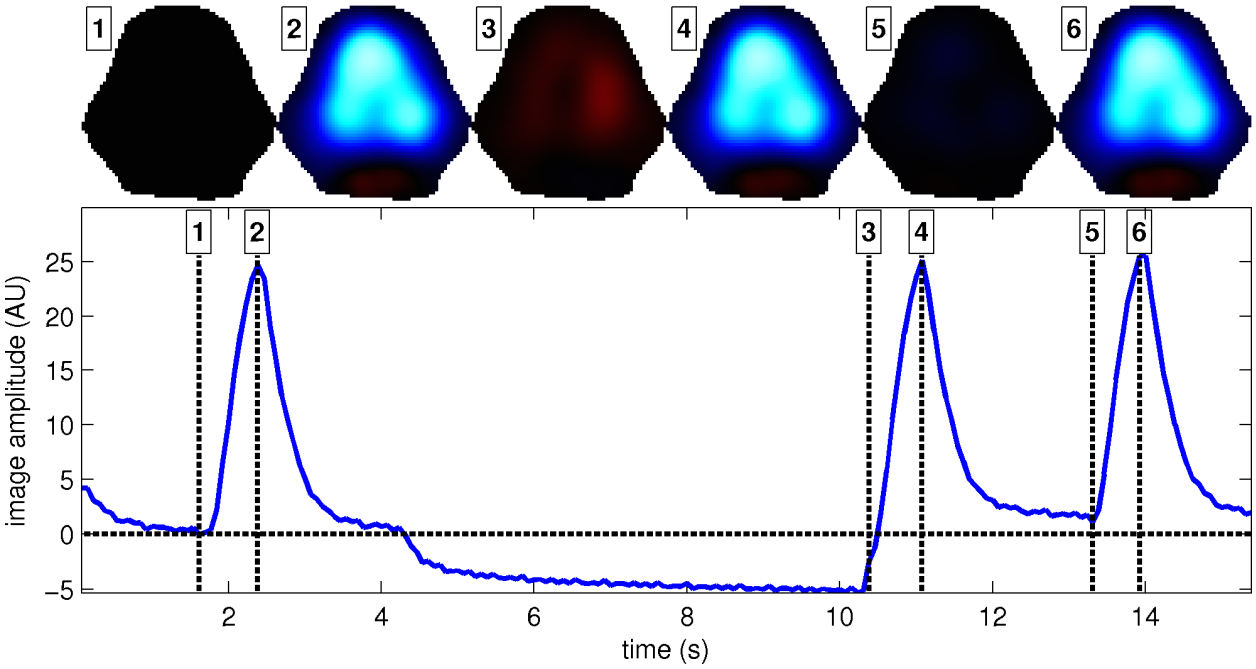

Figure E2.16. EIT images and the global EIT waveform for the "dynamic end-expiratory" baseline measurement, in which the baseline is based on the last three end-expiratory events. Top row, images (using a blue-black-red color coding) corresponding to the indicated times (dashed lines). Bottom row: average image value vs. time for the shown three breaths (data from (3)).

Document preparation

This online document was prepared by A. Adler. It was reviewed and approved by all other authors and collaborators.

References

1. Wilkinson AJ, Randall EW, Cilliers JJ, Durrett DR, Naidoo T, Long T. A 1000-measurement frames/second ert data capture system with real-time visualization. *IEEE Sens J* 2005;5:300-307.
2. Frerichs I, Achtzehn U, Pechmann A, Pulletz S, Schmidt EW, Quintel M, Weiler N. High-frequency oscillatory ventilation in patients with acute exacerbation of chronic obstructive pulmonary disease. *J Crit Care* 2012;27:172-181.
3. Dargaville PA, Rimensberger PC, Frerichs I. Regional tidal ventilation and compliance during a stepwise vital capacity manoeuvre. *Intensive Care Med* 2010;36:1953-1961.
4. Geddes LA, Baker LE. The specific resistance of biological material-a compendium of data for the biomedical engineer and physiologist. *Med Biol Eng* 1967;5:271-293.
5. Faes TJ, van der Meij HA, de Munck JC, Heethaar RM. The electric resistivity of human tissues (100 Hz-10 mHz): A meta-analysis of review studies. *Physiol Meas* 1999;20:R1-10.
6. Halter RJ, Hartov A, Heaney JA, Paulsen KD, Schned AR. Electrical impedance spectroscopy of the human prostate. *IEEE Trans Biomed Eng* 2007;54:1321-1327.
7. Laufer S, Solomon SB, Rubinsky B. Tissue characterization using electrical impedance spectroscopy data: A linear algebra approach. *Physiol Meas* 2012;33:997-1013.
8. Mohr P, Birgersson U, Berking C, Henderson C, Trefzer U, Kemeny L, Sunderkotter C, Dirschka T, Motley R, Frohm-Nilsson M, Reinhold U, Loquai C, Braun R, Nyberg F, Paoli J. Electrical impedance spectroscopy as a potential adjunct diagnostic tool for cutaneous melanoma. *Skin Res Technol* 2013;19:75-83.
9. Murdoch C, Brown BH, Hearnden V, Speight PM, D'Apice K, Hegarty AM, Tidy JA, Healey TJ, Highfield PE, Thornhill MH. Use of electrical impedance spectroscopy to detect malignant and potentially malignant oral lesions. *Int J Nanomedicine* 2014;9:4521-4532.
10. Gabriel C, Peyman A, Grant EH. Electrical conductivity of tissue at frequencies below 1 mHz. *Phys Med Biol* 2009;54:4863-4878.
11. Nopp P, Harris ND, Zhao TX, Brown BH. Model for the dielectric properties of human lung tissue against frequency and air content. *Med Biol Eng Comput* 1997;35:695-702.
12. Proenca M, Braun F, Rapin M, Sola J, Adler A, Grychtol B, Bohm SH, Lemay M, Thiran JP. Influence of heart motion on cardiac output estimation by means of electrical impedance tomography: A case study. *Physiol Meas* 2015;36:1075-1091.
13. Adler A, Guardo R, Berthiaume Y. Impedance imaging of lung ventilation: Do we need to account for chest expansion? *IEEE Trans Biomed Eng* 1996;43:414-420.
14. Coulombe N, Gagnon H, Marquis F, Skrobik Y, Guardo R. A parametric model of the relationship between EIT and total lung volume. *Physiol Meas* 2005;26:401-411.

15. Frerichs I, Braun P, Dudykevych T, Hahn G, Genee D, Hellige G. Distribution of ventilation in young and elderly adults determined by electrical impedance tomography. *Respir Physiol Neurobiol* 2004;143:63-75.

16. Frerichs I, Dudykevych T, Hinz J, Bodenstein M, Hahn G, Hellige G. Gravity effects on regional lung ventilation determined by functional EIT during parabolic flights. *J Appl Physiol* 2001;91:39-50.

17. Heinrich S, Schiffmann H, Frerichs A, Klockgether-Radke A, Frerichs I. Body and head position effects on regional lung ventilation in infants: An electrical impedance tomography study. *Intensive Care Med* 2006;32:1392-1398.

18. Lupton-Smith AR, Argent AC, Rimensberger PC, Morrow BM. Challenging a paradigm: Positional changes in ventilation distribution are highly variable in healthy infants and children. *Pediatr Pulmonol* 2014;49:764-771.

19. Reifferscheid F, Elke G, Pulletz S, Gawelczyk B, Lautenschlager I, Steinfath M, Weiler N, Frerichs I. Regional ventilation distribution determined by electrical impedance tomography: Reproducibility and effects of posture and chest plane. *Respirology* 2011;16:523-531.

20. Riedel T, Richards T, Schibler A. The value of electrical impedance tomography in assessing the effect of body position and positive airway pressures on regional lung ventilation in spontaneously breathing subjects. *Intensive Care Med* 2005;31:1522-1528.

21. Frerichs I, Pulletz S, Elke G, Gawelczyk B, Frerichs A, Weiler N. Patient examinations using electrical impedance tomography-sources of interference in the intensive care unit. *Physiol Meas* 2011;32:L1-L10.

22. Boyle A, Adler A. The impact of electrode area, contact impedance and boundary shape on eit images. *Physiol Meas* 2011;32:745-754.

23. Brown BH, Barber DC, Wang W, Lu L, Leathard AD, Smallwood RH, Hampshire AR, Mackay R, Hatzigalanis K. Multi-frequency imaging and modelling of respiratory related electrical impedance changes. *Physiol Meas* 1994;15 Suppl 2a:A1-12.

24. Smallwood RH, Hampshire AR, Brown BH, Primhak RA, Marven S, Nopp P. A comparison of neonatal and adult lung impedances derived from EIT images. *Physiol Meas* 1999;20:401-413.

25. Adler A, Arnold JH, Bayford R, Borsic A, Brown B, Dixon P, Faes TJ, Frerichs I, Gagnon H, Garber Y, Grychtol B, Hahn G, Lionheart WR, Malik A, Patterson RP, Stocks J, Tizzard A, Weiler N, Wolf GK. Greit: A unified approach to 2D linear EIT reconstruction of lung images. *Physiol Meas* 2009;30:S35-55.

26. Lionheart WR. Eit reconstruction algorithms: Pitfalls, challenges and recent developments. *Physiol Meas* 2004;25:125-142.

27. Bayford RH. Bioimpedance tomography (electrical impedance tomography). *Annu Rev Biomed Eng* 2006;8:63-91.

28. Denai MA, Mahfouf M, Mohamad-Samuri S, Panoutsos G, Brown BH, Mills GH. Absolute electrical impedance tomography (aEIT) guided ventilation therapy in critical care patients: Simulations and future trends. *IEEE Trans Inf Technol Biomed* 2010;14:641-649.

29. Gagnon H, Grychtol B, Adler A. A comparison framework for temporal image reconstructions in electrical impedance tomography. *Physiol Meas* 2015;36:1093-1107.

30. Grychtol B, Elke G, Meybohm P, Weiler N, Frerichs I, Adler A. Functional validation and comparison framework for EIT lung imaging. *PLoS One* 2014;9:e103045.

31. Calderon AP. On an inverse boundary value problem. *Comput Appl Math* 2006;25:133-138.

32. Barber DC, Seagar AD. Fast reconstruction of resistance images. *Clin Phys Physiol Meas* 1987;8 Suppl A:47-54.

33. Santosa F, Vogelius M. A backprojection algorithm for electrical-impedance imaging. *Siam J Appl Math* 1990;50:216-243.

34. Adler A, Guardo R. Electrical impedance tomography: Regularized imaging and contrast detection. *IEEE Trans Med Imaging* 1996;15:170-179.

35. Borsic A, Lionheart WRB, McLeod CN. Generation of anisotropic-smoothness regularization filters for eit. *IEEE Trans Med Imaging* 2002;21:579-587.

36. Borsic A, Graham BM, Adler A, Lionheart WRB. In vivo impedance imaging with total variation regularization. *IEEE Trans Med Imaging* 2010;29:44-54.

37. Grychtol B, Lionheart W, Wolf G, Bodenstein M, Adler A. Impact of model shape mismatch on reconstruction quality in electricalimpedance tomography. *IEEE Trans Med Imaging* 2012; 3:1754-1760.

38. Guardo R, Boulay C, Murray B, Bertrand M. An experimental study in electrical impedance tomography using backprojection reconstruction. *IEEE Trans Biomed Eng* 1991;38:617-627.